Harnessing the Power of Neural Networks for Predicting Shading

Rakeshkumar Mahto* and Kanika Sood†
*Department of Electrical and Computer Engineering
†Department of Computer Science
California State University
Fullerton, California, USA
{ramahto, kasood}@fullerton.edu

2023 IEEE Global Humanitarian Technology Conference (GHTC) | 979-8-3503-2132-6/23/$31.00 ©2023 IEEE | DOI: 10.1109/GHTC56179.2023.10354791

***Abstract*—Unmanned aerial vehicles (UAVs) have emerged as indispensable tools in disaster management, providing critical support in planning, response, and recovery efforts. Integrating photovoltaic (PV) technology with UAVs offers promising opportunities to enhance their functionality and resilience in hostile environments. However, existing PV-based power management systems for UAVs face challenges related to changing light conditions and the impact of partial shading on module performance. It is shown that through embedding transistors with PV panels, the PV based power source of the UAVs can be made adaptable with the operating environment. However, existing shade detection techniques are cumbersome and inefficient.**

In this study, we propose a novel approach using a neural network model to accurately predict the shading percentage on PV cells, enabling dynamic power management. Through extensive experiments, we demonstrate the effectiveness of the model, achieving a high accuracy of 94% with 50 epochs and 96% with 100 epochs. This research highlights the potential of machine learning techniques in optimizing PV-based UAV power systems and provides insights for future advancements in this field. The integration of advanced power management strategies can significantly enhance the performance and adaptability of UAVs, contributing to more efficient and effective disaster response operations.

***Index Terms*—Unmanned aerial vehicles (UAVs), Photovoltaics (PV), neural networks, predictions, disaster management.**

I. Introduction

Recently, unmanned aerial vehicles (UAVs) have emerged as indispensable aids in the aftermath of a natural disaster. They play a vital role in numerous phases of disaster mitigation, from planning and preparation to response and recovery [1]–[3]. In the planning and preparedness phases, UAVs' high-resolution imagery and detailed terrain data are invaluable [4]–[6]. Authorities in charge of preparing for and responding to natural disasters can use this information to create reliable models for assessing risk and implementing efficient action plans. Crucially, such strategies encompass the identification of vulnerable areas, as well as the design of efficient evacuation routes.

UAVs also enhance disaster management systems through their role in predictive warning systems [7]. UAVs equipped with sensors to monitor environmental changes can predict potential disasters, facilitating the transmission of real-time alerts and considerably reducing response times [7]. Moreover, UAVs play a pivotal role in community mobilization during disasters. UAVs can easily access areas that may be hazardous or unreachable for humans and deliver crucial information and relief materials swiftly and effectively [8]–[10]. This expedited assistance is especially critical in the immediate aftermath of a disaster. In the post-disaster phase, UAVs are employed to monitor and evaluate community response effectiveness. They provide detailed, real-time assessments of the extent of damage and the success of response efforts. This invaluable feedback assists in improving disaster management strategies and informs future planning and response tactics. In essence, integrating drones into disaster management systems offers a multi-pronged approach that significantly enhances the effectiveness of disaster response operations.

Although UAVs are increasingly essential in various fields, current models often need to be revised in flight duration, functionality, and resilience to operate in diverse weather conditions. Additionally, while operating in hostile environments such as disaster-hit areas, UAVs need multirole capabilities and resilience to faulty conditions. During disaster assistance missions, the situation evolves unpredictably over time. Therefore, UAVs must possess multirole capabilities to adapt effectively to the dynamic conditions in the field.

Increasing battery capacity is one approach to extending flight time. However, this solution often reduces the payload capacity of the UAV, thereby compromising its functionality [11]. Hydrogen [12]–[14] and gas-powered UAVs [15] are also explored for powering UAVs during natural disaster missions since they provide longer flight endurance and increased payload capacity. However, hydrogen-powered UAVs face safety concerns due to the highly flammable nature of hydrogen, which requires careful handling and storage. Additionally, the limited infrastructure for hydrogen refueling restricts their availability and operational flexibility. Gas-powered UAVs emit pollutants and have higher noise levels, impacting the environment and disrupting rescue operations. As a result, alternative power sources such as photovoltaics (PV) have been extensively explored [16].

While integrating UAVs with PV technology can significantly increase flight duration, the performance of such UAVs is critically dependent on lighting conditions [16]. Moreover, potential damage to a few PV cells in the module due to faults or natural causes can render the UAV nonfunctional. There-

Authorized licensed use limited to: Fresno State Library. Downloaded on August 25,2024 at 20:51:13 UTC from IEEE Xplore. Restrictions apply.

fore, the current power management systems of PV-based UAVs lack the intelligence to adapt in real-time to changing application needs. Moreover, most present-day UAVs utilize PV cells electrically connected in series-parallel (SP) configuration with a parallel-connected bypass diode-based scheme [17]. The performance of such PV-based power sources can significantly decline due to partial and complete shading [18], [19]. If unaddressed, this decline can cause healthy PV cells in the module to become forward-biased, leading them to consume rather than produce electricity. This situation reduces the overall efficiency of the PV module and, in the worst-case scenario, could create hot spots leading to potential fire hazards.

Efficient Maximum Power Point Tracking (MPPT) algorithms have been proposed to mitigate this issue reasonably [20]. However, further research is needed to improve the resilience and efficiency of PV-based UAVs, particularly in their response to changing light conditions and the operational demands of various applications. Since, the MPPT technique is unable to adapt if a couple of PV cells in the panel get damaged while operating in harsh operating conditions.

Studies have demonstrated that incorporating complementary metal-oxide-semiconductor (CMOS) switches into photovoltaic (PV) cells enhances the efficiency of PV modules by mitigating the negative impact of partial shading [21]. CMOS switches allow the PV panel to adapt to changes in shade and faulty conditions. This is done by dynamically reconfiguring the panel's configuration and optimizing power generation by adjusting PV cells in series and parallel [21].

Additionally, CMOS-embedded PV modules can create power islands, facilitating optimal power transfer by matching generated power with load requirements [22]. A computing system, such as the Raspberry Pi, controls the CMOS-embedded PV panel configuration by turning on and off CMOS switches. The computing system utilizes a shade detection algorithm to reconfigure the PV panel, thereby maximizing power generation in various conditions. The algorithm employed for the CMOS embedded PV array incorporates a comparative analysis between computed power and measured power to detect faults [22]. In the event of a fault or shading, the algorithm initiates a scanning process across all rows and columns of the PV module to identify any damaged or shaded cells [22]. Once shaded or faulty PV cells are detected, an optimal configuration for the PV module is calculated and implemented. However, this scanning process and subsequent corrective actions take time to execute. Additionally, the expected power of the PV array is determined using a 1-diode or 2-diode based PV cell modeling technique, which involves a nonlinear mathematical model [23]. Consequently, the computation of expected power becomes challenging, introducing the possibility of inaccurately computed power and triggering the fault detection and mitigation algorithm. Moreover, exponential terms and nonlinearity in the mathematical model make the computation computationally intensive [22].

Sood et al. proposed a machine learning (ML) driven framework for power management in autonomous drones using machine learning [24]. In their work, they conducted a comparative analysis of various ML algorithms, including Support Vector Machines (SVM), Naive Bayes, Random Forest, Voting Classifier, and Decision Trees, to detect shade presence on PV panels [24]. While the detection of shade presence is an important aspect, it is insufficient for effective mitigation of the impact of partial shading conditions. As a result, adding a more thorough analysis of the type and amount of shade on the PV panel can improve the algorithm's capacity to reduce the effects of partial shading conditions. Therefore, this paper aims to enhance the current power management strategy by incorporating a neural network model specifically trained to predict the shading percentage. This work proposes an advanced neural network model for accurately predicting the shading percentage. The neural network is trained on various factors such as temperature, number of PV cells connected in series and parallel, voltage, current, and power generated. We present the model's design, implementation, and validation, along with a comprehensive evaluation of its performance.

The following section describes the dataset used by the neural network model to predict shade presence on the PV cell. Section III elaborates on the neural network techniques employed in the shade percentage prediction model. The results and a detailed description of the neural network model are presented in Section IV. The final section concludes the work and briefly overviews future projects.

II. Dataset

To generate the dataset, we employed a 2-diode based equivalent circuit modeling of PV cells using SPICE, as depicted in Fig. 1 [25]. In this study, we utilized a dataset consisting of 101,580 data points to analyze photovoltaic (PV) panels. The dataset includes PV panel with up to 10 cells in various series-parallel configurations. The temperature of the panels ranges from 27 to 50 °C. We are utilizing the dataset from a previous study, which focused on determining the presence or absence of shading on the PV panels [24]. Thus, the findings of this study can be directly juxtaposed with the results presented in [24], facilitating a comprehensive comparison.

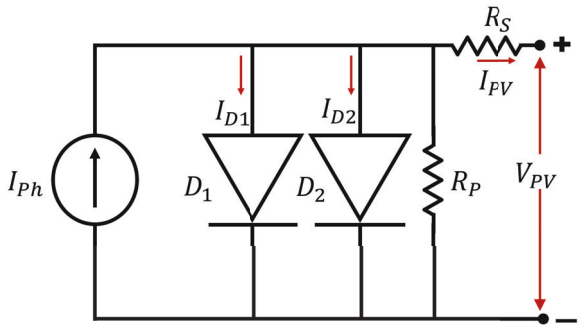

Fig. 1: Equivalent PV cell model utilizing a 2-diode configuration.

Authorized licensed use limited to: Fresno State Library. Downloaded on August 25,2024 at 20:51:13 UTC from IEEE Xplore. Restrictions apply.

$$I_{Ph} = J_{SC} \times A_{PV} \times \frac{G}{G_{SC}} \tag{1}$$

$$I_D = I_S \left[e^{\left(\frac{V_{pv} + I_{pv} \cdot R_S}{A \cdot V_t}\right)} - 1 \right] \tag{2}$$

$$I_{pv} = I_{ph} - I_{D1} - I_{D2} - \left(\frac{V_{pv} + I_{pv} \cdot R_S}{R_P} \right) \tag{3}$$

The photon current (I_{Ph}) in (1) is proportionate to the area of the PV cell's short circuit current, and solar irradiance. Here, J_{SC} represents the short circuit current density in A/cm², A_{PV} denotes the area of the PV cells in cm², G denotes the solar irradiance data (1000 W/m²), and G_{SC} represents the shaded solar irradiance data (500 W/m²). To compute the current flowing from a cell, we use the diode current shown in (2) and (3). The equation considers various factors such as the saturation current (I_S) in amperes, the voltage across a cell (V_{PV}) in volts, the current flowing from a cell (I_{PV}) in amperes, the series resistance (R_S) in ohms, the parallel resistance (R_P) in ohms, the diode ideality constant (A), and the thermal voltage (V_t) in volts.

In the SPICE simulation of the PV cells, we assume a PV cell area of 127 cm², which results in an open circuit voltage of 0.55V and a short circuit current of 2.17A. The saturation current density values for the two diodes, D_1 and D_2, depicted in Fig. 1, are set at 10pA/cm² and 1nA/cm², respectively. Additionally, the equivalent model shown in Fig. 1 has R_S and R_P values of 1mΩ and 100kΩ, respectively. The power vs voltage characteristics of various configurations are shown in Fig. 2a. In Fig. 2a, PV panel is operating under no shade. Meanwhile, Fig. 2b illustrates the power vs voltage characteristics of a PV panel in a 10 x 1 configuration, consisting of 10 PV cells in series and 1 in parallel, under varying shade conditions. When splitting the data, a random 80-20% train-test split was applied, where 20% of the dataset was randomly selected and set aside for the test set.

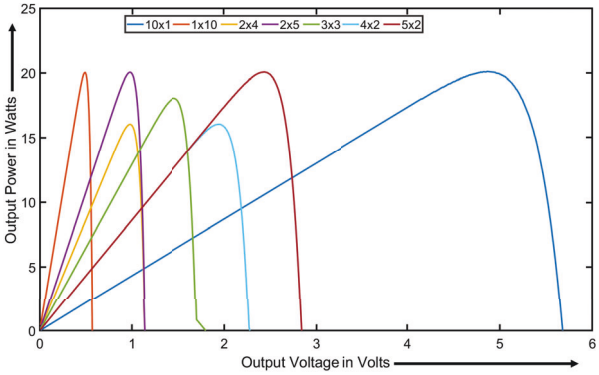

(a)

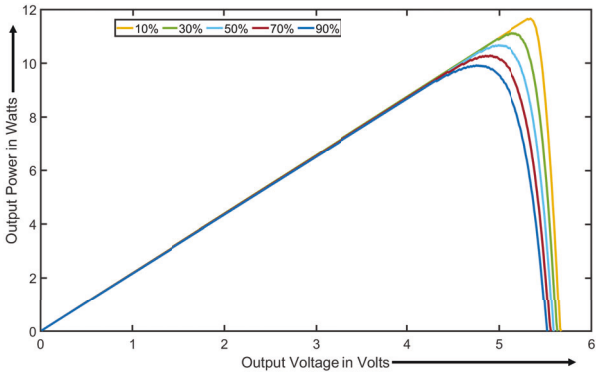

(b)

Fig. 2: a) Power vs Voltage characteristics of PV panel for different configurations (series x parallel) of PV cells b) Power vs Voltage characteristics of PV module in a 10 x 1 configuration under varying shade conditions (10%, 30%, 50%, 70%, and 90% shading)

III. Neural Network Model

In this study, we utilize a range of Python libraries to facilitate data analysis and model development. Key among these are pandas for data handling, numpy for numerical operations, matplotlib and seaborn for data visualization, scikit-learn for data preprocessing and performance metrics, and keras, a high-level neural networks API that runs on top of TensorFlow, for model building and training. The specifics of this network include the following:

A. Input Layer

The input to the model consists of 7 features:

1) Temperature: The feature corresponds to the operating temperature range of PV cells, spanning from 27°C to 50°C.

2) Series: The feature pertains to the arrangement of PV cells using a series-parallel configuration. The numerical value of the feature indicates the number of cells connected in series within the configuration.

3) Parallel: This feature indicates how many PV cells are electrically connected in a parallel setup on the PV panel.

4) Voltage: This feature displays the voltage produced by the PV panel.

5) Current: The feature depicts the current generated by the PV panel.

6) Power: This feature depicts the power generated by the PV panel. The power is equal to output voltage x output current.

These are passed as input neurons to the model. The input layer is the first layer in a neural network which then connects to the intermediatery layers, also known as hidden layers.

B. Hidden Layers

The model consists of three hidden layers. The first two hidden layers have 64 neurons each and use the Rectified

Authorized licensed use limited to: Fresno State Library. Downloaded on August 25,2024 at 20:51:13 UTC from IEEE Xplore. Restrictions apply.

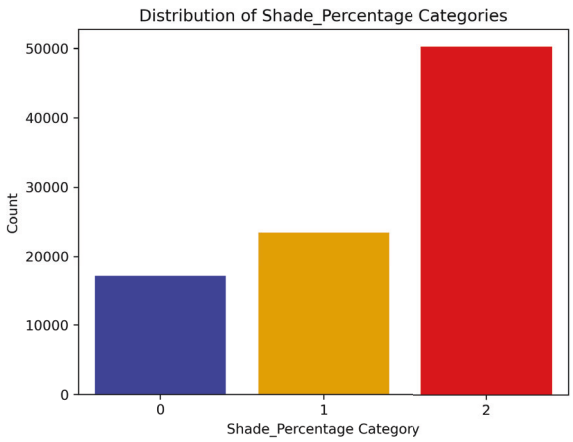

Fig. 3: Distribution of Shade Percentage categories in the dataset: '0' corresponds to high shading percentage, '1' denotes low shading percentage, and '2' represents medium shading percentage.

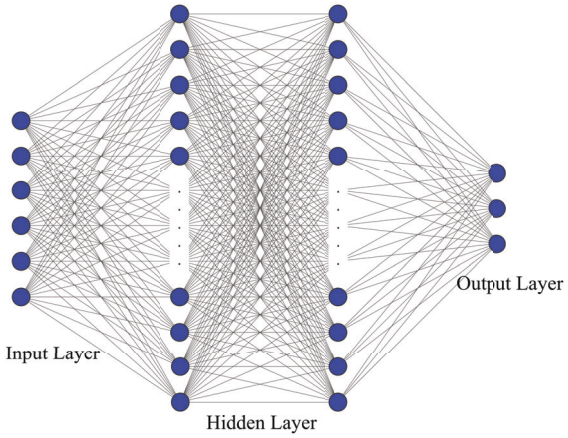

Fig. 4: Neural network architecture illustrating the layers and connections used for shade percentage prediction in PV panels.

Linear Unit (ReLU) activation function. ReLU is often used in the hidden layers because of its efficiency and effectiveness in handling the vanishing gradient problem. These layers are fully connected layers, meaning each neuron in these layers is connected to every neuron in the previous and next layer. To avoid overfitting, we add the hidden layers with a dropout applied at a rate of 0.3. Dropout helps prevent overfitting by providing a way to reduce the complexity and co-adaptations of neurons by ensuring that they work independently. The dropout regularization technique is applied in the hidden layers of the model is represented in (4). Here y is the output of a neuron in the hidden layer, x is the input to that neuron, p is the dropout rate (in this case, 0.3), and m is a binary mask with values 0 or 1. The binary mask m is randomly generated during training, with each element having a probability of (1 - p) of being set to 1 and a probability of p of being set to 0. Dropout is a regularization technique where randomly selected neurons are ignored during training. This means that their contribution to the activation of downstream neurons is temporarily removed on the forward pass and any weight updates are not applied to the neuron on the backward pass.

$$y = \left(\frac{m \cdot x}{1-p}\right) \tag{4}$$

C. Output Layer

The shade percentage depicts the number of PV cells under different shading levels, ranging from 10%, 20%, 30%, 40%, 50%, 60%, 70%, 80%, 90%, to 100% shading of PV panels. Later, the shading percentages are further categorized as "low" for 0% to 20% shading, "medium" for shading between 21% to 80%, and "high" for shading between 81% to 100%. The distribution of PV cells across these shading categories is shown in Fig. 3. The category of "medium" shading has a more considerable amount of data compared to the other categories due to the inclusion of shading percentages ranging from 21% to 80%. This broader range encompasses a significant portion of the dataset, resulting in a higher concentration of data points within the "medium" shading category, as shown in Fig. 3.

The output layer of the model uses the softmax activation function and has 3 neurons. The softmax activation function is used in the output layer of the model [26] is defined in (5).

$$softmax(z)_i = \left(\frac{e^{Z_i}}{\Sigma_{j=1}^{N} e^{Z_j}}\right) \tag{5}$$

Where Z_i represents the input to the i^{th} neuron in the output layer, N is the total number of neurons in the output layer. This equation showcases how the softmax activation function transforms the input values into a probability distribution across the different output classes (low, medium, and high shade percentages). The resulting probabilities indicate the likelihood of a data point belonging to each class.

Each of these neurons represents a class of shade percentage (low, medium, and high). The shade percentage is as follows: 0-20 % low, 21-80 % medium, and 81-100 % high. These are classified as class labels: 0, 1 and 2 for high, low, and medium. The softmax activation function is a generalization of the logistic function that "squashes" a K-dimensional vector of arbitrary real values into a K-dimensional vector of real values in the range [0, 1] that add up to 1. This means that the output of this layer can be interpreted as the probabilities of a data point belonging to each class.

D. Model Compilation and Performance Metrics

The model is compiled with the 'Adam' optimizer and 'categorical_crossentropy' loss. Adam is an optimization algorithm that can be used instead of the classical stochastic gradient descent procedure to update network weights iterative based on training data. Categorical cross entropy is a loss function that is used for single-label categorization tasks where each data point belongs to exactly one class. It's used as a loss for multi-class

Authorized licensed use limited to: Fresno State Library. Downloaded on August 25,2024 at 20:51:13 UTC from IEEE Xplore. Restrictions apply.

classification problems. We use multiple standard performance metrics for assessing the performance of the model. These metrics include (1) overall accuracy, (2) confusion matrix, (3) precision (4) recall (5) F-1 score.

The accuracy metrics are used for assessing the performance of the model. This is simply the proportion of correct predictions made by the model. Overall accuracy is one of the useful measures when the target variable classes in the data are nearly balanced. In every epoch of training, the accuracy of the model on the training data and validation data is calculated and reported. The confusion matrix looks into the correct and incorrect predictions for each class label. This ensures even with class imbalance we assess the built model fairly. The precision is the ratio of true positives to all predicted positives (true positives and false positives) and is used to test how well a model avoids false positives. The recall also known as the true positive rate (TPR), is the ratio of correctly classified instances for the positive class as well as the total samples for that class. The F-1 score is the ratio as provided below:

$$F1score = \left(\frac{2 \cdot Precision \cdot Recall}{Precision + Recall}\right) \tag{6}$$

In the next section, we provide a detailed report of each of these metrics on the test set.

IV. Results and Discussion

To assess the effectiveness of the proposed neural network model, a comprehensive evaluation is conducted utilizing various evaluation metrics and visualization techniques. This approach allows for a thorough analysis of the model's performance. The subsequent subsections present detailed results obtained from the evaluation, including an assessment of model accuracy, a scatter plot representation, and the analysis of the confusion matrix at both 50 and 100 epochs.

Firstly, the model's accuracy is measured to gauge its ability to correctly predict shade percentages. The accuracy metric is tracked during the training process for both the training and testing datasets. The results, depicted in Fig. 5 a) and b), demonstrate the progression of accuracy with each epoch for both datasets. At 50 epochs, the model achieves a training accuracy of 93.3%, indicating its proficiency in learning the patterns within the training data. Correspondingly, the testing accuracy is 93.55%, highlighting the model's ability to generalize well on unseen data. Upon further training until 100 epochs, the model's performance improves, with a training accuracy of 96.55% and a testing accuracy of 95.91% shown in Fig. 5a and Fig. 5b, respectively.

Furthermore, a confusion matrix analysis is conducted to evaluate the model's performance in classifying shade percentage categories. The confusion matrix provides a comprehensive overview of the predicted shade percentage distribution compared to the actual categories. At 50 epochs, the confusion matrix reveals the distribution of predictions for each shade percentage category as shown in Fig. 6a. Similarly, at 100 epochs, the confusion matrix provides a comprehensive analysis of the model's classification accuracy for each category is shown in Fig. 6b.

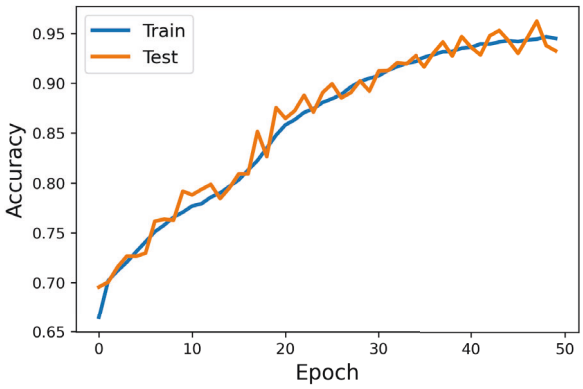

(a)

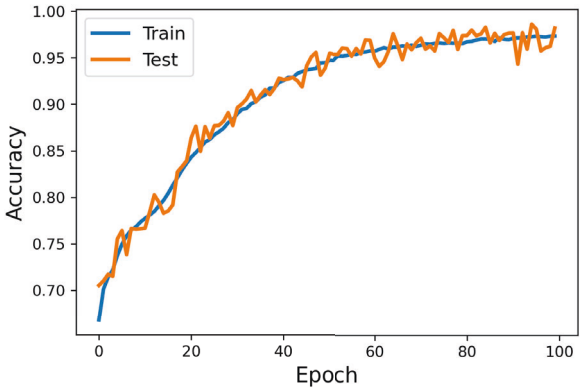

(b)

Fig. 5: Model Accuracy Progression for a) 50 Epochs and b)100 Epochs)

A plot illustrating the results obtained from training the implemented neural network model is presented in Fig. 7a and 7b. The plot illustrates the performance of the model in terms of accuracy across 50 epochs and 100 epochs.

As the training progresses, the model exhibits a notable improvement in accuracy. After 50 epochs, the model achieves 94%, 95%, and 93% precision rates for the low, medium, and high shading categories, respectively, as shown in, as shown in Fig. 7a. Further training up to 100 epochs increases the precision to 82%, 97%, and 96% for the respective shading categories, as illustrated in Fig. 7a. These results emphasize the effectiveness of the neural network model in accurately predicting the shading percentage as training iterations increase. The plot provides valuable insights into the model's convergence and performance, demonstrating its ability to adapt and learn from the dataset over time. The observed trend indicates that increasing the number of epochs enhances the model's accuracy, highlighting the significance of continued training for improved predictions.

Authorized licensed use limited to: Fresno State Library. Downloaded on August 25,2024 at 20:51:13 UTC from IEEE Xplore. Restrictions apply.

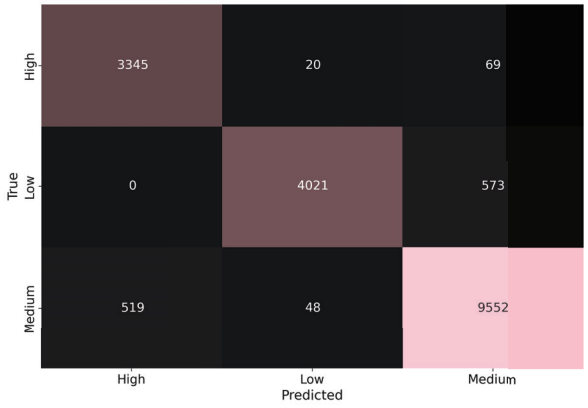

(a)

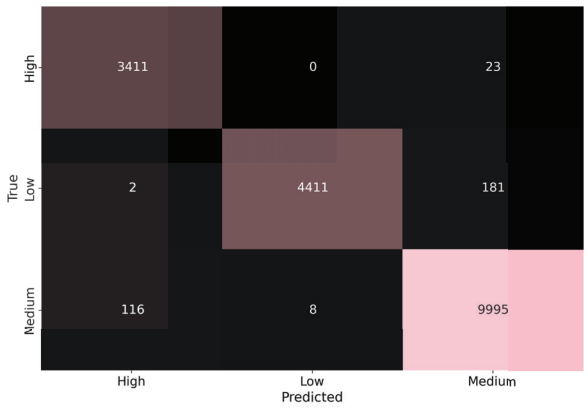

(b)

Fig. 6: Confusion matrix for a) 50 Epochs b) 100 Epochs

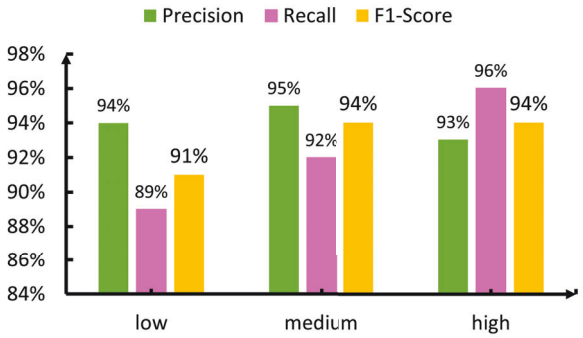

(a)

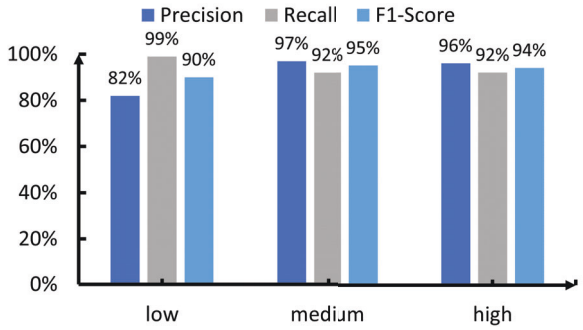

(b)

Fig. 7: Classification report for a) 50 Epochs b) 100 Epochs

These findings establish the effectiveness and reliability of the proposed neural network model for accurately predicting the shading percentage in PV panels. The increasing precision with additional epochs suggests the potential for achieving even higher performance with extended training durations. Additionally, a scatter plot is employed to visually represent the relationship between power and voltage within the dataset. As illustrated in Fig. 7, the scatter plot offers insights into potential trends or clusters within the data. Each data point is color-coded based on the shade percentage category it belongs to, with ”high” shading percentage represented in blue, ”less” shading percentage in orange, and ”medium” shading percentage in red. This visual representation aids in discerning any discernible patterns or groupings among the data points, allowing for a deeper understanding of the relationships between power, voltage, and shade percentage.

By conducting these evaluations and analyses, a comprehensive understanding of the model's performance is obtained. The results obtained from the accuracy assessment, scatter plot analysis, precision, F-1 score, recall, and confusion matrix analysis highlight the effectiveness and robustness of the proposed neural network model in accurately predicting shade

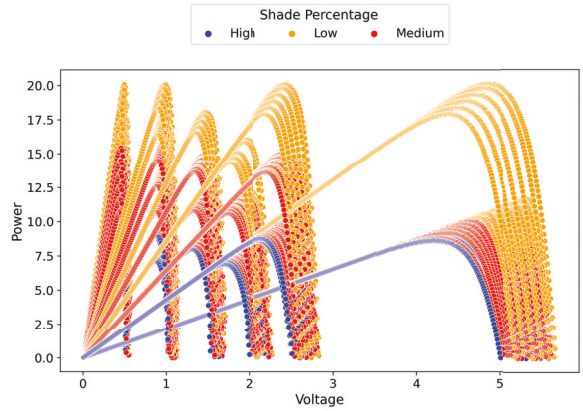

Fig. 8: Scatter plot of power vs. voltage with shading percentage.

percentages.

V. Conclusion

The proposed neural network model has shown promising results, surpassing traditional methods and opening avenues for more advanced power management strategies in autonomous drones. By integrating this model into the power management system, we aim to enhance drones' sustainability and operational endurance, enabling them to operate effec-

Authorized licensed use limited to: Fresno State Library. Downloaded on August 25,2024 at 20:51:13 UTC from IEEE Xplore. Restrictions apply.

tively in diverse and challenging environments. Artificial intelligence and machine learning algorithms allow for dynamic adaptation to the operating conditions, further optimizing the power management capabilities of UAVs.

This research contributes to the ongoing discourse on technological advancements in drone applications and using renewable energy sources. It highlights the potential of machine learning techniques in optimizing and managing power in autonomous drones, showcasing their applicability in various domains. Furthermore, the proposed technique holds promise for application in space exploration, offering potential solutions for powering satellites.

This work focused on temperature variations within the range of 27°C to 50°C; however, there is potential for future research to investigate the behavior of the proposed neural network model under even more extreme temperature conditions. The findings and insights gained from such an investigation will be reported in a separate article, providing a comprehensive analysis of the model's performance across a broader temperature range. This expanded research would contribute to a deeper understanding of power management in autonomous drones, enabling their effective operation in a broader range of environmental conditions.

In conclusion, this work demonstrates the efficacy of the proposed neural network model. It sets the stage for future advancements in power management for autonomous drones, fostering sustainable and efficient operations in challenging environments.

ACKNOWLEDGMENT

This work is fully supported by the Research Alliance Seed Grant Program of NSF-ADVANCE Partnership Grant (NSF ID 2121950)-Kindling Inter-university Networks for Diverse Engineering Faculty Advancement in the California State University System.

REFERENCES

[1] S. Li et al., "Drones and Other Technologies To Assist in Disaster Relief Efforts," Tennessee. Department of Transportation, 2022.

[2] A. Khan, S. Gupta, and S. K. Gupta, "Emerging UAV technology for disaster detection, mitigation, response, and preparedness," Journal of Field Robotics, vol. 39, no. 6, pp. 905–955, 2022.

[3] S. Grogan, R. Pellerin, and M. Gamache, "The use of unmanned aerial vehicles and drones in search and rescue operations–a survey," Proceedings of the PROLOG, pp. 1–13, 2018.

[4] T. Schlurmann, W. Kongko, N. Goseberg, D. H. Natawidjaja, and K. Sieh, "Near-field tsunami hazard map Padang, West Sumatra: Utilizing high resolution geospatial data and reseasonable source scenarios," in Proceedings of the Coastal Engineering Conference (2010), Reston: American Society of Civil Engineers, 2010.

[5] M. Rusnák, J. Sládek, A. Kidová, and M. Lehotskỳ, "Template for high-resolution river landscape mapping using UAV technology," Measurement, vol. 115, pp. 139–151, 2018.

[6] M. W. Ewertowski, A. M. Tomczyk, D. J. Evans, D. H. Roberts, and W. Ewertowski, "Operational framework for rapid, very-high resolution mapping of glacial geomorphology using low-cost unmanned aerial vehicles and structure-from-motion approach," Remote Sensing, vol. 11, no. 1, p. 65, 2019.

[7] M. Erdelj, E. Natalizio, K. R. Chowdhury, and I. F. Akyildiz, "Help from the sky: Leveraging UAVs for disaster management," IEEE Pervasive Computing, vol. 16, no. 1, pp. 24–32, 2017.

[8] Z. Wenjian, Z. Sidong, C. RongJie, X. Jingchang, L. Yeqian, and C. Huiru, "Design of a relief materials delivery system based on UAV," in IOP Conference Series: Materials Science and Engineering, IOP Publishing, 2020, p. 012049.

[9] Y. Huang, H. Han, B. Zhang, X. Su, and Z. Gong, "Supply distribution center planning in UAV-based logistics networks for post-disaster supply delivery," in 2020 IEEE International Conference on E-health Networking, Application & Services (HEALTHCOM), IEEE, 2021, pp. 1–6.

[10] M. A. R. Estrada and A. Ndoma, "The uses of unmanned aerial vehicles–UAV's-(or drones) in social logistic: Natural disasters response and humanitarian relief aid," Procedia Computer Science, vol. 149, pp. 375–383, 2019.

[11] W. Jaafar and H. Yanikomeroglu, "Dynamics of Laser-Charged UAVs: A Battery Perspective," IEEE Internet of Things Journal, vol. 8, no. 13, pp. 10573–10582, Jul. 2021, doi: 10.1109/JIOT.2020.3048087.

[12] C. De Wagter et al., "The NederDrone: A hybrid lift, hybrid energy hydrogen UAV," international journal of hydrogen energy, vol. 46, no. 29, pp. 16003–16018, 2021.

[13] O. Bingöl and B. Özkaya, "Analysis and comparison of different PV array configurations under partial shading conditions," Solar Energy, vol. 160, pp. 336–343, 2018.

[14] D. Kramer, "Hydrogen-powered aircraft may be getting a lift," Physics Today, vol. 73, no. 12, pp. 27–29, 2020.

[15] B. Heater, "MIT's gas-powered drone is able to stay in the air for five days at a time," TechCrunch, Jun. 27, 2017. https://techcrunch.com/2017/06/27/mits-gas-powered-drone-is-able-to-stay-in-the-air-for-five-days-at-a-time/ (accessed May 30, 2023).

[16] S. A. H. Mohsan, M. A. Khan, F. Noor, I. Ullah, and M. H. Alsharif, "Towards the Unmanned Aerial Vehicles (UAVs): A Comprehensive Review," Drones, vol. 6, no. 6, Art. no. 6, Jun. 2022, doi: 10.3390/drones6060147.

[17] W. Zhou and K. Jin, "Optimal Photovoltaic Array Configuration Under Gaussian Laser Beam Condition for Wireless Power Transmission," IEEE Transactions on Power Electronics, vol. 32, no. 5, pp. 3662–3672, May 2017, doi: 10.1109/TPEL.2016.2583502.

[18] F. Belhachat and C. Larbes, "A review of global maximum power point tracking techniques of photovoltaic system under partial shading conditions," Renewable and Sustainable Energy Reviews, vol. 92, pp. 513–553, 2018.

[19] I. R. Balasubramanian, S. Ilango Ganesan, and N. Chilakapati, "Impact of partial shading on the output power of PV systems under partial shading conditions," IET power Electronics, vol. 7, no. 3, pp. 657–666, 2014.

[20] Y. Chu, C. Ho, Y. Lee, and B. Li, "Development of a Solar-Powered Unmanned Aerial Vehicle for Extended Flight Endurance," Drones, vol. 5, no. 2, Art. no. 2, Jun. 2021, doi: 10.3390/drones5020044.

[21] R. V. Mahto, D. K. Sharma, D. X. Xavier, and R. N. Raghavan, "Improving performance of photovoltaic panel by reconfigurability in partial shading condition," Journal of Photonics for Energy, vol. 10, no. 4, pp. 042004–042004, 2020.

[22] R. V. Mahto, Fault resilient and reconfigurable power management using photovoltaic integrated with CMOS switches. The University of New Mexico, 2016.

[23] N. Barth, R. Jovanovic, S. Ahzi, and M. A. Khaleel, "PV panel single and double diode models: Optimization of the parameters and temperature dependence," Solar Energy Materials and Solar Cells, vol. 148, pp. 87–98, 2016.

[24] K. Sood, R. Mahto, H. Shah, and A. Murrell, "Power Management of Autonomous Drones using Machine Learning," in 2021 IEEE Conference on Technologies for Sustainability (SusTech), Apr. 2021, pp. 1–8. doi: 10.1109/SusTech51236.2021.9467475.

[25] L. Castañer and S. Silvestre, Modelling Photovoltaic Systems Using PSpice. John Wiley and Sons, 2002.

[26] R. A. Dunne and N. A. Campbell, "On the pairing of the softmax activation and cross-entropy penalty functions and the derivation of the softmax activation function," in Proc. 8th Aust. Conf. on the Neural Networks, Melbourne, Citeseer, 1997, p. 185.

Authorized licensed use limited to: Fresno State Library. Downloaded on August 25,2024 at 20:51:13 UTC from IEEE Xplore. Restrictions apply.